A Comprehensive Modeling of Dynamic Negative-Bias Temperature Instability in PMOS Body-Tied FinFETs

Hyunjin Lee, *Student Member, IEEE,* Choong-Ho Lee, Donggun Park, *Senior Member, IEEE,*
and Yang-Kyu Choi, *Member, IEEE*

***Abstract*—This paper presents a novel approach to estimate the rising and falling behavior of Nth-order ON-state current by dynamic negative-bias temperature instability (DNBTI), with a comparison between experimental data and a modified DNBTI model in PMOS body-tied FinFETs for the first time. The modified model was proposed to predict not only Nth-order DNBTI behavior but also temperature and stress bias effects. The fin-width dependence was analyzed, and different trends between silicon-on-insulator and body-tied FinFETs were explained with the extracted DNBTI model parameters: stress time, oxide-field strength, and temperature. The proposed model closely matched the measured static lifetime.**

***Index Terms*—Body tied, double gate, dynamic negative-bias temperature instability (DNBTI), FinFET, floating-body, reliability, silicon-on-insulator (SOI).**

I. INTRODUCTION

MULTIGATE FinFET structures are promising nanoscale devices having features of high robustness on short-channel effects and excellent scalability using conventional processes [1], [2]. As the device is scaled down, the negative-bias temperature instability (NBTI) starts to limit the device reliability of digital and analog CMOS circuits [3], [4]. Previous studies indicate an improvement to the negative-bias-temperature (NBT) stress with a wide fin width in silicon-on-insulator (SOI) and body-tied FinFETs [5], [6]. Recently, a recovery of the NBTI has become a concern for the ac-lifetime prediction of the device [7], [8]. In this paper, dynamic-NBTI (DNBTI) reliabilities of fully depleted body-tied PMOS FinFETs were investigated and modeled through a new approach with consideration of stress biases (V_{st}), fin widths (W_{Fin}), body temperatures (T), and -0.2 V substrate biases (V_{sub}).

II. EXPERIMENTS

Negative biases ($V_G = V_{\mathrm{TO}} - V_{\mathrm{st}},\ V_{\mathrm{TO}} = V_G$ at $I_D = -100$ nA and $V_D = -50$ mV) for stress states and positive biases ($V_G = V_{\mathrm{TO}} + V_{\mathrm{st}}$) for recovery states were applied to body-tied FinFET gates. Additionally, the source/drain and the substrate were grounded with various values of T: 50 °C, 80 °C, 125 °C, and 150 °C. A V_{sub} of -0.2 V was applied to certify the virtual-floating-body effects of SOI FinFETs, which was similar to a previous study [4]. Detailed fabrication processes have already been reported [2]. To interpret the failure mechanisms of DNBTI, a change of the ON current ($I_{\mathrm{ON}} = I_D$ at $V_G - V_{\mathrm{TO}} = -1$ V and $V_D = -1$ V) after the stresses and the electrochemical-reaction models at the Si/SiO$_2$ interface [9], [10] were used.

III. RESULTS AND DISCUSSIONS

Fig. 1 shows the DNBTI degradation and enhancement with various values of V_{st}, T, W_{Fin}, and V_{sub}. An I_{ON} degradation on the stress state represents an increment of the interface state (N_{it}) and the oxide-trap charge (N_{ot}) by Si–H bond breaking; furthermore, its enhancement on the recovery state represents N_{ot} neutralization and N_{it} repassivation. A V_{st} increment induced more holes at the interface, broke more Si–H bonds in stress states, and promoted more rediffused hydrogenated species for N_{it} and more accumulated electrons for N_{ot} in recovery states [7], [11]. An increment of T weakened the Si–H bonds in stress states and expedited rediffusion of repassivation species in recovery states. A W_{Fin} reduction induced more holes in stress states and more passivated N_{ot} due to accumulated electrons in recovery states. An increment of the hole concentration by accumulated electrons at the center of the fin due to virtually floating-body ($V_{\mathrm{sub}} = -0.2$ V) is dominant in the low-oxide-field (E_{ox}) condition [5]. In contrast, a decrease of hole concentration from the substrate to the gate is dominant in high-E_{ox} condition due to negative V_{sub} in stress states [12]. More electrons were induced at the interface due to forwardly biased substrate in recovery states. For an analytical and comprehensive understanding of DNBTI with V_{st}, T, W_{Fin}, and V_{sub}, the previous model [10] was revamped with the introduction of a fitting parameter κ to describe the cyclic I_{ON} variation in Fig. 1 as follows:

$$\Delta I_{\mathrm{ON}} = A\kappa t^n (E_{\mathrm{ox}})^m \exp\left(-\frac{E_a}{k_B T}\right) \tag{1}$$

Manuscript received September 19, 2005. This work was supported in part by Samsung Electronics Company, Ltd. and in part by the Korea Ministry of Science and Technology under the National Research Program for the 0.1-Tb Nonvolatile Memory Development. The review of this letter was arranged by Editor S. Chung.

H. Lee and Y.-K. Choi are with the Department of Electrical Engineering and Computer Science, Korea Advanced Institute of Science and Technology, Daejeon 305-701, Korea (e-mail: jinlee@eeinfo.kaist.ac.kr).

C.-H. Lee and D. Park are with Device Research, Semiconductor R&D Division, Samsung Electronics Company, Kyunggi-Do 449-711, Korea.

Digital Object Identifier 10.1109/LED.2006.870864

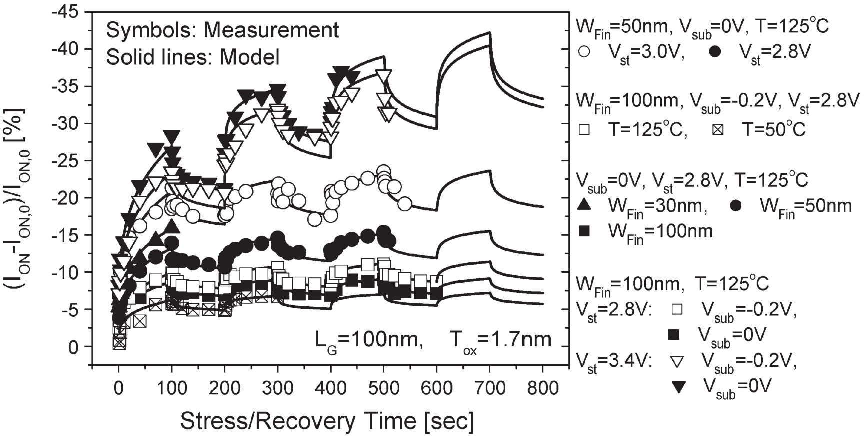

Fig. 1. $\Delta I_{\mathrm{ON}}/I_{\mathrm{ON},0}$ of DNBTI versus stress/recovery time with various V_{st}, T, W_{Fin}, and V_{sub}. Solid lines represent the modeled DNBTI profiles using the proposed method, which was an attractive approach to predict the Nth-order stress/recovery profiles.

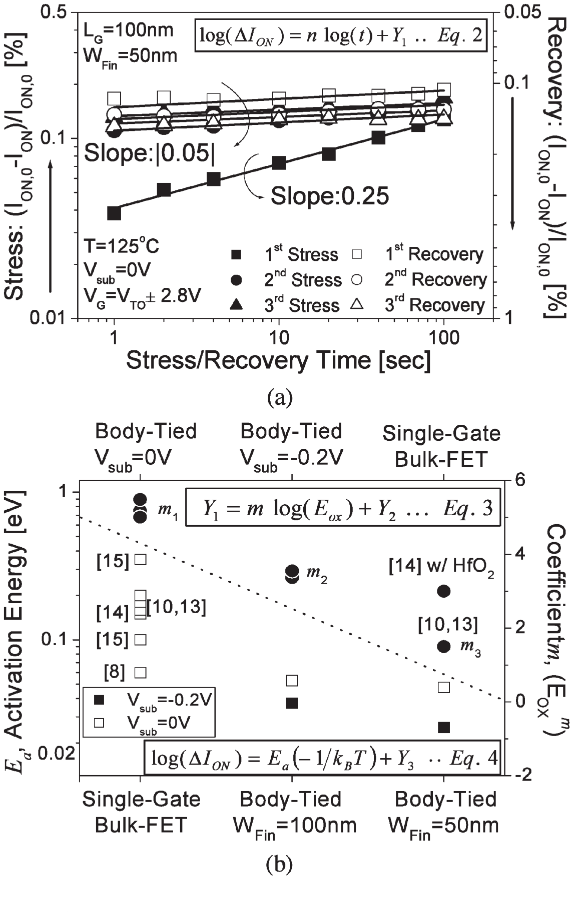

(a)

(b)

Fig. 2. (a) I_{ON} degradation and enhancement with a number of stress and recovery states. First stress n is fixed to 0.25 and reduced to ±0.05 after the first recovery and the second stress. (b) Right and top axis shows m with a single-gate and body-tied FinFET ($V_{\mathrm{sub}} = 0$ and -0.2 V). Left and bottom axis shows E_a of body-tied FinFETs with W_{Fin} values of 50 nm and 100 nm and a single-gate bulk FET (infinite W_{Fin}).

TABLE I

EXTRACTED COEFFICIENTS A, n, m, AND E_a AFTER THE FIRST STRESS WITH $W_{\mathrm{Fin}} = 50$ nm, 100 nm AND $V_{\mathrm{sub}} = 0$ V, -0.2 V. E_a SHOWS W_{Fin} DEPENDENCE, AND A, m, AND E_a SHOW V_{sub} DEPENDENCE

W_{Fin}	V_{sub}	A	n	m	E_a
100nm	**0V**	**2×10^{-37}**	**0.25 ±0.05**	**5**	**0.053eV**
	-0.2V	**1×10^{-26}**	**0.25 ±0.05**	**3.5**	**0.037eV**
50nm	**0V**	**2×10^{-37}**	**0.25 ±0.05**	**5**	**0.048eV**
	-0.2V	**1×10^{-26}**	**0.25 ±0.05**	**3.5**	**0.025eV**
Bulk FET	-	-	**0.25**	**1.5**	**0.06eV~ 0.35eV**

where A is a proportional factor to tailor the order of magnitude of I_{ON}; t is the stress time, i.e., aging time; and E_a is the activation energy of the holes to break Si–H bonds.

Fig. 2(a) shows I_{ON} variation on stress and recovery states versus stress/recovery time. n is the exponent for the time dependence and extracted from Eq. 2 in the inset of Fig. 2(a). After the first stress, n was 0.25 and was then reduced to ±0.05 after the first recovery and the second stress. The + sign corresponds to stress states and the − sign corresponds to recovery states. The coefficient $n = 0.25$ comes from the diffusion mechanism [9], [10], and the reduction of n ($= \pm 0.05$) comes from the lock-in mechanism [7]. This reduction was caused by insufficiently passivated N_{it} or N_{ot} due to the lost hydrogenated species during the first stress. The exponent n was independent of W_{Fin}, V_{st}, T, and V_{sub}. Fig. 2(b) shows the extracted m from Eq. 3 in the inset of Fig. 2(b), the exponent for the E_{ox}, such as m_1 ($V_{\mathrm{sub}} = 0$ V, FinFET); m_2 ($V_{\mathrm{sub}} = -0.2$ V, FinFET); and m_3 (single gate). m did not show W_{Fin} dependence, but it showed V_{sub} dependence. m increased as the number of gates increased, i.e., $m_{1,2} > m_3$ [10], [14]. In the inset of Fig. 2(b), Eq. 4 was used to extract E_a, which was larger in the single-gate bulk planar MOSFET than the body-tied FinFETs [8], [10], [13]–[15]. E_a decreased as W_{Fin} decreased and a negative V_{sub} was applied. Table I summarizes the extracted coefficients: A, n, m, and E_a after the first stress. The virtual floating-body, $V_{\mathrm{sub}} = -0.2$ V, indicated the decrement of m and E_a. Thus, NBTI was worse at an SOI than at a bulk substrate, which was consistent with the previous report [5].

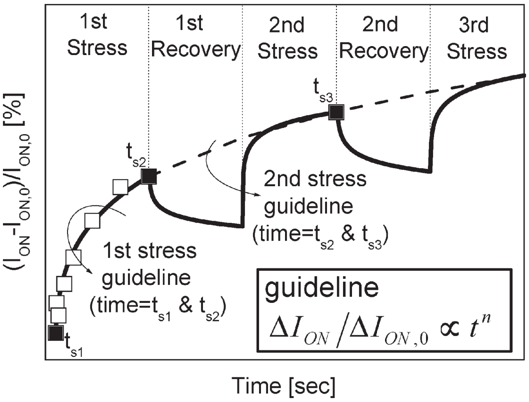

Fig. 3. Periodic $\Delta I_{\mathrm{ON}}/I_{\mathrm{ON},0}$ under DNBT stress. The first stress guideline increased according to t^n with $n = 0.25$ and changed to $n = 0.05$ at the second guideline.

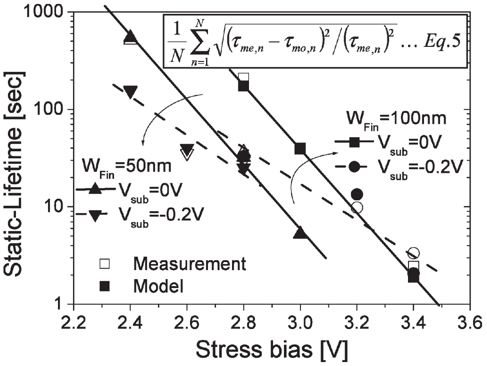

Fig. 4. Measured and modeled static lifetimes at $W_{\mathrm{Fin}} = 50$ nm, 100 nm and $V_{\mathrm{sub}} = 0$ V, -0.2 V versus V_{st} according to (1) and the parameters in Table I. The root-mean-square error is 16%.

Fig. 3 shows an estimation of the I_{ON} variation using the measured data under the DNBT stress. Guidelines of $\Delta I_{\mathrm{ON}}/I_{\mathrm{ON},0}$ under the NBT stress increased according to the power law t^n, while the guideline after the first stress was extracted from t_{s1} to t_{s2} with $n = 0.25$. Additionally, the I_{ON} variation between t_{s2} and t_{s3} was predicted a second stress guideline with $n = 0.05$ [16]. The solid lines of Fig. 1 represent the modeled DNBTI profiles using the proposed method, which was an attractive approach to predict the Nth-order stress or the recovery with V_{st} and T. Periodic stress and recovery profiles are well explained using (1), the parameters in Table I, the first and second guidelines, and the fitting parameter κ. Fig. 4 shows the static lifetime predicted by the model versus V_{st}. A measured lifetime (τ_{me}) and a modeled lifetime (τ_{mo}) were compared, and the root-mean-square error using Eq. 5 in the inset of Fig. 4 was 16%.

IV. CONCLUSION

A modified DNBTI model and an extraction method were developed to predict the Nth-order DNBTI profile with various V_{st}, T, W_{Fin}, and V_{sub}. The stress-time exponent n was 0.25 at the first stress state and was changed to ±0.05 after the first recovery state. A decrement of E_a with a narrower W_{Fin} represented the increment in N_{it} and device degradation. A virtual floating-body indicated a decrement of the coefficient m and E_a. The modeled static lifetime coincided well with the measured static lifetime showing root-mean-square error of 16%.

REFERENCES

[1] Y.-K. Choi, N. Lindert, P. Xuan, S. Tang, D. Ha, E. Anderson, T.-J. King, J. Bokor, and C. Hu, "Sub-20 nm CMOS FinFET technologies," in *IEDM Tech. Dig.*, Washington, DC, 2001, pp. 421–424.

[2] T. Park, S. Choi, D. H. Lee, J. R. Yoo, B. C. Lee, J. Y. Kim, C. G. Lee, K. K. Chi, S. H. Hong, S. J. Hyun, Y. G. Shin, J. N. Han, I. S. Park, U. I. Chung, J. T. Moon, E. Yoon, and J. H. Lee, "Fabrication of body-tied FinFETs (Omega MOSFETs) using bulk Si wafer," in *Symp. VLSI Tech. Dig.*, Kyoto, Japan, 2003, pp. 135–136.

[3] V. Reddy, A. T. Krishnan, A. Marshall, J. Rodriguez, S. Natarajan, T. Rost, and S. Krishnan, "Impact of negative bias temperature instability on digital circuit reliability," in *Proc. Annu. Int. Reliability Physics Symp.*, Dallas, TX, 2002, pp. 248–254.

[4] C. Schliinder, R. Brederlow, B. Ankele, A. Lill, K. Coser, and R. Thewes, "On the degradation of p-MOSFETs in analog and RF circuits under inhomogeneous negative bias temperature stress," in *Proc. Annu. Int. Reliability Physics Symp.*, Dallas, TX, 2003, pp. 5–10.

[5] H. Lee, C.-H. Lee, D. Park, and Y.-K. Choi, "Negative bias temperature instability study of sub-40nm SOI and body-tied FinFETs," *IEEE Electron Device Lett.*, vol. 26, no. 5, pp. 326–328, May 2005.

[6] H. Kufluoglu and M. A. Alam, "A geometrical unification of the theories of NBTI and HCI time-exponents and its implications for ultra-scaled planar and surround-gate MOSFETs," in *IEDM Tech. Dig.*, San Francisco, CA, 2004, pp. 113–116.

[7] S. Rangan, N. Mielke, and E. C. C. Yeh, "Universal recovery behavior of negative bias temperature instability," in *IEDM Tech. Dig.*, Washington, DC, 2003, pp. 341–344.

[8] V. Huard and M. Denais, "Hole trapping effect on methodology for DC and AC negative bias temperature instability measurements in PMOS transistors," in *Proc. Annu. Int. Reliability Physics Symp.*, Phoenix, AZ, 2004, pp. 40–45.

[9] C. E. Blat, E. H. Nicollian, and E. H. Poindexter, "Mechanism of negative-bias-temperature instability," *J. Appl. Phys.*, vol. 69, no. 3, pp. 1712–1720, Feb. 1991.

[10] S. Ogawa and N. Shiono, "Generalized diffusion-reaction model for the low-field charge-buildup instability at the $\mathrm{Si-SiO_2}$ interface," *Phys. Rev. B, Condens. Matter*, vol. 51, no. 7, pp. 4218–4230, Feb. 1995.

[11] S. Tsujikawa, K. Watanabe, R. Tsuchiya, K. Ohnishi, and J. Yugami, "Experimental evidence for the generation of bulk traps by negative bias temperature stress and their impact on the integrity of direct-tunneling gate dielectrics," in *Symp. VLSI Tech. Dig.*, Kyoto, Japan, 2003, pp. 139–140.

[12] M.-G. Chen, J.-S. Li, C. Jiang, C. H. Liu, K.-C. Su, and Y.-J. Chang, "NBTI mechanism explored on the back gate bias for pMOSFETs," in *Proc. Integrated Reliability Workshop*, Lake Tahoe, CA, 2003, pp. 131–132.

[13] G. Haller, M. Knoll, D. Braunig, F. Wulf, and W. R. Fahrner, "Bias–temperature stress on metal–oxide–semiconductor structures as compared to ionizing irradiation and tunnel injection," *J. Appl. Phys.*, vol. 56, no. 6, pp. 1844–1850, Sep. 1984.

[14] M. Houssa, M. Aoulaiche, S. V. Elshocht, S. D. Gendt, G. Groeseneken, and M. M. Heyns, "Negative bias temperature instabilities in HfSiON/TaN-based pMOSFETs," in *IEDM Tech. Dig.*, San Francisco, CA, 2004, pp. 121–124.

[15] N. Kimizuka, K. Yamaguchi, K. Imai, T. Iizuka, C. T. Liu, R. C. Keller, and T. Horiuchi, "NBTI enhancement by nitrogen incorporation into ultrathin gate oxide for 0.10-μm gate CMOS generation," in *Symp. VLSI Tech. Dig.*, Honolulu, HI, 2000, pp. 92–93.

[16] Y. Mitani, "Influence of nitrogen in ultra-thin SiON on negative bias temperature instability under AC stress," in *IEDM Tech. Dig.*, San Francisco, CA, 2004, pp. 117–120.